# Visualizing MR Diffusion Tensor Fields by Dynamic Fiber Tracking and Uncertainty Mapping

Hans-H. Ehricke, Uwe Klose, and Wolfgang Grodd

**Corresponding Author:**

Prof. Dr.sc.hum. Hans-Heino Ehricke

Fachhochschule Stralsund

Institut für Angewandte Informatik

Zur Schwedenschanze 15

D-18435 Stralsund

Fax: (+49)3831-456687

Phone: (+49)3831-456674

hans.ehricke@fh-stralsund.de

Coauthors:

Dr. rer. nat. habil. Uwe Klose

Prof. Dr.med.habil. Wolfgang Grodd

Universitästklinikum Tübingen

Section Exp. MR of the CNS

Abteilung für Neuroradiologie

Hoppe-Seyler-Str. 3

D-72076 Tuebingen

EHRICKE, H-H., U. KLOSE und W. GRODD: *Visualizing MR Diffusion Tensor Fields by Dynamic Fiber Tracking and Uncertainty Mapping.* Computers and Graphics, 30:255-264, 2006.

# Visualizing MR Diffusion Tensor Fields by Dynamic Fiber Tracking and Uncertainty Mapping

Hans-H. Ehricke[a,*], Uwe Klose[b], and Wolfgang Grodd[b]

[a] Computer Graphics Lab, University of Applied Sciences, Stralsund, Germany; [b] Section of Experimental NMR of the CNS, University Hospitals, Tübingen, Germany

**Abstract**—Recent advances in magnetic resonance imaging have provided methods for the acquisition of high-resolution diffusion tensor fields. Their 3D-visualization with streamline-based techniques - called fiber tracking - allow analysis of cerebral white matter tracts for diagnostic, therapeutic as well as neuro-scientific purposes. The illusiveness of fiber visualizations and the inability to reliably visualize branching structures are problems still waiting for solutions. In this paper we present an on-the-fly approach to the tracking of branching and crossing fibers by dynamically setting secondary seeds in regions where branching is assumed, thus avoiding computationally intensive preprocessing steps. Moreover, we propose an uncertainty mapping technique which uses color coding to enrich 3D fiber displays with information on their validity. Probability values for fiber samples are computed from dataset features as well as characteristics of the tracking process. In contrast to data optimization and pre-processing approaches, our algorithms focus on highly interactive visualization scenarios in collaborative environments.

**Keywords:** Tracking; Medical information systems; Interaction techniques

* Corresponding Author, Tel. (+49)3831-456674, Fax (+49)3831-383085

# 1 INTRODUCTION

In Magnetic Resonance Imaging (MRI) in-vivo measurement of the anisotropic behaviour of water diffusion has become possible. By Diffusion Tensor Imaging (DTI) this behaviour is decribed with a 3D second-order tensor field (see appendix). Since in cerebral white matter the principally random motion of water molecules is restricted by axonal membranes and myelin sheats, diffusion anisotropy allows depiction of directional anisotropy within neural fiber structures. Due to the huge amount of information inherent in diffusion tensor fields, their 3D visualization is a highly complex task requiring strategies of information condensation. Apart from very few approaches for direct volume rendering [1], the great majority of proposed DTI visualization techniques focus on the integration of sample points along fiber trajectories and their three-dimensional depiction [2]. These streamline-based approaches are called fiber tracking. They usually make use of the principal eigenvector of the diffusion ellipsoid as an estimate of the predominant direction of water diffusion in a voxel. It could be demonstrated that with these techniques the in-vivo investigation and visualization of fiber tracts in concordance with existing knowledge of white-matter anatomy has become feasible, thus opening up completely new perspectives for neurological research as well as practical applications, such as neurosurgery planning.

By streamline-based fiber tracking and visualization, highly impressive images may be generated and presented to researchers and physicians. However, due

to deficiencies of the tracking algorithm and shortcomings inherent in the datasets (noise, artefacts, partial voluming), they may be illusive by depicting fiber tracts which do not exist in reality or by missing to visualize important connectivity features, e.g. branching structures. In order to avoid misinterpretations, the viewer of the visualizations must be provided with some information on the uncertainty of a depicted fiber and of its presence in a certain location. In this paper we propose a probability estimation algorithm and a colour coding scheme for uncertainty mapping, allowing fiber visualizations to be enriched with information from the dataset as well as the tracking process. Regarding connectivity, we tackle the problem of analyzing branching trajectories with a recursive tracking algorithm, based on the idea of dynamically setting new seed points during tracking.

## 2 RELATED WORK

In the context of flow visualization a variety of methods for the visualization of 3D-vector fields have been proposed. Many of them use particle tracing techniques, starting from seedpoints, in order to visualize the field's directional structure by integral curves. Zöckler et al. use texture mapping features of the graphics hardware to illuminate the resulting streamlines [3]. Additionally, the rendered streamlines are enriched by color coding, applying color to depict some scalar quantity, e.g. the vector magnitude. Zang et al. use stream tubes to visualize white matter tracts from DTI datasets [4]. While the trajectory of each

tube sweeps along the principal eigenvector field, additional tensor field information is depicted by the tube's shape and colour. The cross-sectional shape is an ellipse representing the ratio of the second and third eigenvectors, whereas the colour shows the linear anisotropy value. A similar approach is proposed by McGraw et al. [5].

DTI fiber tracking algorithms commonly use the principal eigenvectors as estimates of the fiber orientation and the linear diffusion anisotropy values at each voxel in order to guide the tracking process. Within an interactively defined region of interest (ROI) seed points are selected at voxels where a pre-defined anisotropy threshold is reached. For each seed point a fiber is tracked in both directions by following the local vector orientation. If we step from voxel to voxel using the discrete vector at each voxel, the tracked line will increasingly differ from the ideal line with each further step. Therefore, a more continuous approach is required. The general solution for vector field integration is the Runge-Kutta approach allowing estimation of the next sample on the line by computing a weighted average of vector orientations [6]. Mori et al. propose the FACT (fiber assignment by continuous tracking) method which traces the line on a subvoxel level, linearly interpolating the principal eigenvectors as well as the anisotropy values from the neigbouring voxels [7]. The tracking stops when (1) the sample point does not reach the anisotropy threshold or (2) the sample's vector orientation differs by more than a pre-defined angle from the previous vector. This strategy is used to avoid the generation of non-realistic connections and the tracking of fibers which do not

exist in reality. However, even the usage of high thresholds cannot ensure the production of absolutely correct results [8]. This is due to mainly two deficiencies of the DTI data: Noise and limited spatial resolution. Low signal to noise ratio (SNR) is a great handicap for fiber tracking. Coulon et al. propose a field regularisation technique for principal eigenvector diffusion fields [9,10]. They use partial differential equations to model the realtionships between neighbouring vectors and regularize vector orientations in an iterative manner. Poupon et al. base their regularization technique on a low curvature hypothesis for fascicles [11]. They use a Bayesian framework together with a global model of the likelihood of a fascicle direction map in order to compute a regularized direction map. Pasternak et al. propose to use a multiple diffusion tensor approach [12]. Their regularization algorithm results with multiple orientations describing each voxel. Thus, crossing fibers in a voxel may be tracked by usage of the corresponding vector. Limited spatial resolution is responsible for the fact, that usually a fiber voxel contains not only one, but a whole bunch of axons. This is not a problem, when axons run in parallel. However, in branching structures which are common with cerebral white matter anatomy, the diffusion tensors no longer represent a linear anisotropy with a distinct principal eigenvector. The cigar-like shape of the tensor degenerates to a disk shape. This means, that the first and second eigenvectors have similar lengths, and therefore we cannot determine a distinct predominant direction in the voxel. The tensorlines approach uses the incoming vector from the last tracking step as an estimate and deflects it according to the tensor's shape in the current

voxel [13]. If the shape is a disk, the incoming vector is not deflected, thus substituting the voxel's principal eigenvector by the vector from the last tracking step. If the shape is more cigar-like, the vector is deflected in direction of the tensor's principal eigenvector. Another method to tackle the branching problem is the exhaustive search approach [14]. Here, tracking is initiated using all brain voxels as seed candidates, generating a great number of fiber lines. Only those fibers which penetrate the branching region of interest are kept. This avoids the necessity of splitting a line into two, but is computationally very expensive. A similar approach with seeds that are evenly distributed over the volume is proposed in [15]. Since in branching/crossing voxels the orientations of eigenvectors are highly uncertain, exhaustive search fiber tracking may produce wrong connections.

Few approaches can be found in the literature tackling the problem of the validity of fiber visualizations. As mentioned above, in [4] and [5] a streamtubes technique is used for fiber visualization allowing mapping of local anisotropy features to the tube's shape and colour. In [16] the uncertainty of detected surfaces is visualized by point based primitives. Uncertainty is mapped to the displacement of points which are used to render the surface.

## 3 SYSTEM OVERVIEW

### 3.1 Data acquisition and preparation

The DTI measurements were performed with a conventional 3 Tesla whole body MR scanner (Magnetom Trio, Siemens Medical Solutions, Erlangen, Germany). Resolution of the acquired data volumes was 1 mm in plane with a

slice thickness ranging from 1.3 to 2.0 mm. We used diffusion weighting in six directions [17]. The six diffusion sensitizing gradient orientations along the main gradient axes [Gx, Gy, Gz] were [1,1,0], [1,0,1], [0,1,1], [-1,1,0], [0,-1,1], [1,0,-1].

From the MR scanner the data was transferred to a Linux workstation where slice shifts were restored by a motion correction procedure. Next, the data volumes were interpolated to a spatial resolution of 0.5x0.5x1.0 $mm^3$. For each voxel the tensor matrix was computed, and from this parameters characterizing the diffusion ellipsoid: (1) The direction of the principal eigenvector, (2) the standard deviation of the three eigenvalues and (3) the normalized difference $\Delta_{12} = (\lambda_1 - \lambda_2) / (\lambda_1 + \lambda_2 + \lambda_3)$ between the largest two eigenvalues.

**3.2 Visualization**

For the purpose of tracking and visualization the data was transfered to a Virtual Reality (VR) System, consisting of (1) a passive stereo-display with backprojection, driven by two high-resolution beamers, (2) a Windows-PC equipped with a nVidia Quadro4 900XGL graphics accelerator (NVIDIA Corporation, Santa Clara) and (3) an optical tracking system including a flystick (ARTTtrack1 and Dtrack, ART GmbH, Munich). We use amiraDev, amiraVR and OpenInventor (all Mercury Computer Systems Inc., Chelmsford) as data processing and visualization tools. Our tracking and uncertainty mapping algorithms were implemented with C++ as amira modules and integrated in the amira framework. This allowed us to immediately evaluate data and algorithms

within a highly interactive environment. We use VR technology in order to communicate ideas in our interdisciplinary team of computer scientists, radiologists, surgeons and physicists (fig. 1).

## 4 DYNAMIC SEED TRACKING (DST) APPROACH

### 4.1 Detecting branches

As explained above, branching structures and their correct interpretation and visualization are one of the key problems of fiber tracking. Limited spatial resolution of the DTI data is the principal reason: The diameter of a single axon is in the order of micrometers, whereas the resolution of diffusion MRI is limited to one or several millimeters. Thus, a fiber voxel in general will contain more than a single axon. If a trajectory branches or two fibers cross each other, a voxel may contain axons with different orientations. The resulting tensor cannot be used for the determination of fiber orientations, because the underlying model for tensor calculation is based on the assumption of linear anisotropic diffusion in a preferred direction. Therefore, in branching regions neither the principal, nor the other two eigenvectors can be used for fiber propagation. However, we can use the fact, that the eigenvalues $\lambda_1$ and $\lambda_2$ of the principal and second eigenvectors do not differ much, in order to recognize a branching or crossing situation. Another possibility of detecting fiber branches is the analysis of vector deviations in the local environment of a sample along the tracked fiber. If the sample's interpolated eigenvector differs by more than a certain angle from the previous vector, we have a high probability for a branching situation. Instead of analyzing the angle, it is easier to use its cosine, which can

easily be computed by the inner product of the two normalized eigenvectors $\varepsilon_1$ and its predecessor $\varepsilon_{1,prev}$:

$$R = abs(\varepsilon_1 \cdot \varepsilon_{1,prev})$$

We use the absolute value of the inner product, because for fiber tracking only the orientation of linear anisotropy possesses relevance, not its direction. Equally, we can analyze the principal eigenvector orientations of the sample's 8 neighbour voxels. As a quantitative measure the parameter $R'$ can be calculated as the sum of the inner products of the vectors [7]:

$$R' = 1/56 \sum_{i=1..8} \cdot \sum_{j=1..8, i \neq j} abs(\varepsilon_{1,i} \cdot \varepsilon_{1,j})$$

where $\varepsilon_{1,i}$ and $\varepsilon_{1,j}$ are the normalized eigenvectors of the neighbouring voxels. In regions with low vector conformity $R'$ becomes small and the probability of branching or crossing fibers is high. The choice of $R$ or $R'$ as a vector conformity criterium is a parameter specified by the user.

### 4.2 Dynamic seed tracking algorithm

The DST algorithm we present here is based on the FACT method (see above). Within an interactively defined seed region, voxels are selected as starting points for fiber tracking. Instead of the standard deviation of eigenvalues, we use the normalized difference $\Delta_{12}$ as an anisotropy measure. All voxels within the seed region which reach a threshold $\Delta_{12,T}$ are selected as seeds. We follow the fiber trajectory in both directions by using linearly interpolated eigenvector orientations and sampling the dataset with subvoxel resolution, e.g. *steplength* = 0.25 x *voxelsize*. Two user-defined thresholds are used to determine a sample's

validity: Both, the anisotropy threshold $\Delta_{12,T}$ and the vector conformity threshold $R_T$ must be reached in order to accept the sample as a fiber point. Here, $R_T$ is the criterium for the analysis of neighbouring vector orientations on the basis of the inner product value $R$ or $R'$. If the condition is not met, the tracking of the fiber stops. The principal idea of our algorithm is that, if we are confronted with a stop situation, we analyze the local environment in order to detect and follow fiber branches or crossings. For this purpose we store the coordinates of the sample which has caused the discontinuity, adding it to a stop sample list. After all the seeds from the primary seed region have been processed, we return to the stop sample list and apply to each sample a secondary tracking algorithm which is described by the flowchart in fig. 2.

Fig. 3 illustrates the mechanism of the DST algorithm with a crossing (left) and a branching (right) structure. The two squares represent slices through the center of a secondary seedbox, constructed around the stop sample. The arrows show the eigenvector orientations. The dark shading marks voxels which have already been tracked and accepted as fiber points. Voxels with stars are seeds for secondary fiber tracking. Those voxels which are accepted as members of new fibers touching the center voxel, have been shaded with light gray colour. The two examples show that the region around a stop sample is analyzed and processed, producing secondary fibers when there are branches or crossings. Requesting a secondary fiber to touch the center voxel of the seedbox ensures, that we accept new fibers, only if they have a connection to the original stop

sample and the corresponding primary fiber. Of course, the new fibers do not really penetrate the center voxel, because the general threshold conditions for fiber tracking are used also for secondary tracking, and they were not fulfilled by the stop sample located at the seedbox center. It is obvious that, if we do not use the "*center voxel fiber condition*" and accept all fibers which originate from the seedbox, a lot of new fibers are produced in the neighbourhood of each stop sample. Since the algorithm works recursively, allowing stop samples to be added to the stop sample list, also when tracking a secondary fiber, such a strategy would result in a whole bunch of fibers around the original seed region, including crossing and branching structures. This might be useful e.g. in situations where the overall white matter connectivity in a certain brain region is to be studied. A compromise between these two strategies is to force secondary fibers to touch a sphere of a certain size around the original stop sample. Increasing the sphere diameter from voxelsize to seedbox size allows the user to vary tracking parameters and produce more fibers.

**4.3 Results of DST**

The dynamic seed tracking approach was evaluated by investigating 2 patient-, 3 volunteer- and 1 phantom-study. As a phantom we used boiled asparagus with different placing schemes in a water tank. In the volunteer studies we focused on the investigation of cerebellar tracts. Fig. 4 presents a result from a healthy volunteer dataset. The primary seed region was defined near the brainstem and allowed visualization of one of the main tracts, called inferior cerebellar peduncle. The left image shows a surface display of the brainstem

(gray) together with the streamline visualization of the inferior cerebellar peduncle (red), produced by tracking without dynamic seeding. The middle and right images illustrate the effect of the DST algorithm: Crossing fibers from the superior cerebellar peduncle as well as additional branches of the inferior cerebellar peduncle have been tracked and visualized (middle, yellow). In this case, secondary fibers were only accepted when touching the center voxel of a seedbox. The right image illustrates the result of using all fibers within the secondary seedbox. Fig. 5 also gives an example of a DST application where all fibers originating from a seedbox are accepted as secondary fibers. The data is from the case of a brain tumor patient. The image shows an integrated 3D-display of orthogonal slices through the anisotropy volume, ventricular system (violet) and tumor (blue) as surface displays as well as the fibers as red coloured streamlines.

## 5 UNCERTAINTY MAPPING

In neurology in-vivo measurement and 3D-visualization of cerebral fiber pathways are becoming important tools for diagnostic and therapeutic procedures. E.g. in cases of cerebral neoplasms it is important to know, whether the tumor disrupts or only compresses fiber tracts and which tracts - connecting which regions - are affected and maybe damaged by surgery [18,19]. It is therefore of vital importance that fiber visualization methods produce images without illusive visualizations. However, due to the deficiencies inherent in the DTI datasets as well as algorithmic problems, we cannot produce images which are fully reliable. E.g. if we increase the anisotropy and vector conformity

thresholds for tracking, we may enlarge the probability, that a fiber we have found, exists in reality. On the other hand, by this strategy we also enlarge the probability of missing fibers, parts of fibers as well as fiber branches. Therefore, it is necessary to supply the viewer with additional information, allowing estimation of how reliable the presented information is. With our uncertainty mapping approach we enrich streamlines with validity information, representing the probability that a certain fiber point really exists. We have experimented with different mapping techniques. Rendering streamlines with point primitives and mapping probability values to the opacity and/or density of points did not yield convincing visual results, due to the high anatomic complexity of the scenes. With a colour coding mechanism much better results could be achieved. The probability value of a certain fiber location can be mapped to colour scale and used as an index into a colour map. The fiber point is colourized with the corresponding colour during rendering. More complex is the problem of computing appropriate probability values. One possibility would be the usage of dataset features, such as anisotropy values (normalized difference $\Delta_{12}$ of the first two eigenvalues) and local conformity of eigenvector orientations $R$ or $R'$. They have to be mapped to the probability scale [0..1] and may be combined in order to compute a local probability $P_{loc,i}$ at a certain sample $i$:

$$P_{loc,i} = a \cdot P_{a,loc,i} + (1-a) \cdot P_{\varepsilon,loc,i}$$

where:

$$P_{a,loc,i} = m_1 \cdot \Delta_{12}$$

$$P_{\varepsilon,loc,i} = m_2 \cdot R \quad bzw. \quad P_{\varepsilon,loc,i} = m_2 \cdot R'$$

*a* is a weighting factor in the range from 0 to 1, $m_1$ and $m_2$ are scaling factors.

### 5.1 Mapping global tracking features

However, the consideration of only local features seems not sufficient for an appropriate probability computation scheme. If we arrive at a certain sample point during tracking and accept it as a fiber member, this is not only dependent on local dataset features. The uncertainty of a fiber at the sample very much depends on the path we have tracked so far, regarding all the decisions which have been made on this way. So, the local probability must be weighted with a global measure, representing the overall probability of the fiber path. Thus we compute the sample's conditional probability. In order to find a solution, the following consideration may be helpful: If we arrive at a sample point with a low local probability and accept it as a fiber member, the likelihood of the following path segments becomes low. That means that the conditional probabilities of subsequent samples cannot be higher than those of their predecessors, even if they possess high local probabilities. A solution which obeys to these conditions is given by the following formula:

$$P_{path,i} = P_{cond,i} = P_{loc,i} \cdot P_{path,i-1}$$

where $P_{path,i}$ and $P_{path,i\text{-}1}$ are the overall path probabilities at sample *i* and *i*-1,

respectively and $P_{cond,i}$ is the conditional probability of sample $i$. If we use $P_{cond,i}$ for colour mapping of fiber streamlines, we can supply the viewer with information about dataset features as well as characteristics of the tracking algorithm.

**5.2 Results**

As stated above, we investigated 6 datasets in order to evaluate our approach. Fig. 6 illustrates a result from the cerebellar dataset, introduced above. Here, we applied our DST method to the tracking of the inferior cerebellar peduncle and its branches, using slightly higher thresholds for anisotropy as well as vector conformity. The left image shows the result of local uncertainty mapping with the vector conformity $R$ as the only feature. We apply a hue ramp ranging from blue to red as a color map, thus visualizing probability differences with high contrast. On the right side the conditional probability was used by weighting the local probability with the overall path probability. Fiber segments with high uncertainty (blue to green) can easily be identified and distinguished from segments with high probability (yellow to red). In fig. 7 the effect of uncertainty mapping is demonstrated by visualizing fibers from the brain tumor dataset. Here, we used the standard deviation of eigenvalues and the vector conformity $R$ for local probability computation and mapped the conditional probability values to the fiber streamlines. This allowed visualization of fibers and their probabilities in the neighbourhood of the tumor. In the image on the right the tumor surface (blue) was removed in order to visualize fibers at its back. For the presented datasets tracking as well as probability mapping processing took less than 0.5 seconds/frame on a standard 1,7 Ghz. Intel CPU.

## 6 SUMMARY AND CONCLUSION

We have presented algorithms for a DTI data analysis approach, enabling highly interactive visualization scenarios in collaborative environments, as an alternative or complement to highly-complex data optimization and pre-processing schemes. We have introduced an interactive realtime method to tracking branching and crossing fibers. In contrast to state-of-the-art approaches we avoid computationally intensive pre-processing steps which either are based on vector field regularization mechanisms or generate a multitude of fibers from seedpoints distributed over the whole volume. Moreover, we have presented an uncertainty mapping technique allowing viewers of 3D fiber displays to estimate fiber uncertainty. We do not only use local features for probability computation, but propose a global likelihood scheme taking into account features along tracked fiber paths. Although we could achieve good results with 6 datasets, further evaluation of the method on the basis of synthetic data and phantom studies is necessary. In this context the robustness of the approach has to be evaluated, particularly with regard to the great number of parameters which have to be specified by the user.

Our preliminary results suggest that with uncertainty mapping and dynamic fiber tracking the practical relevance of DTI acquisition and visualization may be enhanced. From future advances in imaging technology we can expect higher-quality data with better spatial resolution and higher SNR, thus augmenting the value of the method for diagnostic and therapeutic procedures. The transfer from the research laboratory to clinical practice will require

optimized interaction techniques on the visualization part of the method. Currently, fiber visualization from tensor fields is a highly interactive process, requiring the collaboration of physicians and computer scientists, e.g. for the definition of seed regions, the specification of tracking and rendering parameters, the segementation and reconstruction of object surfaces, the construction of the scene from object surfaces, slice images, streamlines, the evaluation of visualization results and many more. From our experience a virtual reality system with stereoscopic wide angle display and head/device tracking makes it easier to directly interact with scene objects, e.g. seedboxes, and allows a faster and more comprehensive analysis of DTI vector fields. However, in a clinical environment we usually do not have available virtual reality systems operated by interdisciplinary staffs. Therefore, the optimization of interaction schemes for the visualization of DTI data will be a key subject of further investigations. We are convinced that by focussing on special purpose applications, such as neurosurgery planning, practical solutions may be provided in the near future.

## APPENDIX: DIFFUSION TENSOR IMAGING FUNDAMENTALS

The random, thermally driven motion of water molecules (water diffusion) may be quantified my MR imaging. By applying magnetic field gradients in different directions we can sensitize molecules and measure directionally dependant motion. In brain white matter, diffusion is anisotropic, because water molecules are hindered from freely moving in directions orthogonal to axonal orientations by membranes and myelin sheats. Therefore, the principal direction of diffusion is along axonal fibers. By the quantification of anisotropic diffusion we can gather information on fiber orientation in a voxel. The diffusion tensor is a 3x3 matrix of values representing the DTI measurements with different diffusion sensitizing gradients:

$$D = \begin{pmatrix} D_{xx} & D_{xy} & D_{xz} \\ D_{yx} & D_{yy} & D_{yz} \\ D_{zx} & D_{zy} & D_{zz} \end{pmatrix}$$

Since the diffusion tensor is diagonally symmetric ($D_{ij} = D_{ji}$), only six values are independent and the matrix is fully determined by these six parameters. Therefore, usage of six diffusion sensitizing gradient orientations is sufficient for DTI measurement. If we increase their number, we may improve measurement accuracy. From the tensor we can estimate the diffusivity in any arbitrary direction or we may determine the direction of maximum diffusivity.

Usually we describe anisotropic water diffusion by an ellipsoid model which we fit to the tensor matrix (fig. 8). The ellipsoid's orientation is characterized by

three eigenvectors $E = (\varepsilon_1, \varepsilon_2, \varepsilon_3)$. Its shape is determined by the corresponding eigenvalues $(\lambda_1, \lambda_2, \lambda_3)$. These paramters are computed from the tensor matrix by diagonalization, such that:

$$D = E^T \begin{pmatrix} \lambda_1 & 0 & 0 \\ 0 & \lambda_2 & 0 \\ 0 & 0 & \lambda_3 \end{pmatrix} E$$

$\varepsilon_1$ is the principal eigenvector representing the direction of maximum diffusivity (fig. 9). The corresponding anisotropy value is $\lambda_1$. We can characterize the degree of linear anisotropy present in a voxel, by the standard deviation of the three eigenvalues.

If a voxel is part of a fiber tract, we usually find a high standard deviation. We can estimate fiber orientation by $\varepsilon_1$. If the voxel contains axons with different orientations, e.g. in branching or crossing structures, the difference between $\lambda_1$ and $\lambda_2$ becomes small and the ellipsoid has a disk-like shape. In this case, fiber orientations cannot be determined by the tensor's eigenvectors.

## REFERENCES


[1] G. Kindlmann, D. Weinstein, and D. Hart, "Strategies for Direct Volume Rendering of Diffusion Tensor Fields," IEEE Trans. Visualization Comp. Graph., vol. 6, pp. 124 - 138, Apr. - Jun. 2000.

[2] S.Mori, and P.C.M. van Zijl, "Fiber Tracking: Principles and Strategies - a Technical Review," NMR Biomed., vol. 15, pp. 468 - 480, 2002.

[3] M. Zöckeler, D. Stalling, and H.-C. Hege, "Interactive Visualization of 3D-Vector Fields Using Illuminated Streamlines," *Proc. IEEE Visualization 96*, pp. 107 - 113, 1996.

[4] S. Zhang, C. Demiralp, and D.H. Laidlaw, "Visualizing Diffusion Tensor MR Images Using Streamtubes and Streamsurfaces," IEEE Trans. Visualization Comp. Graph., vol. 9, pp. 454 - 462, Oct.. - Dec. 2003.

[5] T. McGraw, B.C. Vemuri, Y.Chen, M. Rao, T. Mareci, DT-MRI Denoising and Neuronal Fiber Tracking, Med Im Analysis, vol. 8, pp 95-111, 2004.

[6] D. Stalling, H.C. Hege, Fast and Resolution Independent Line Integral Convolution, In: Proc. SIGGRAPH 95, pp. 249-256, 1995.

[7] S. Mori, B.J. Crain, V.P. Chacko, and P.C.M. van Zijl, "Three-Dimensional Tracking of Axonal Projections in the Brain by Magnetic Resonance Imaging," Annals Neurolog., vol. 45, pp. 265 - 269, 1999.

[8] C. Pierpaoli, A.S. Barnett, S. Pajevic, A. Virta, and P.J. Basser, "Validation of DT-MRI Tractography in the Descending Motor Pathways of Human Subjects," *Proc. Intl. Soc. Mag. Reson. Med. 9,* p. 501, 2001.

[9] O. Coulon, D.C. Alexander, and S.R. Arridge, "A Regularization Scheme for

Diffusion Tensor Magnetic Resonance Images," *Information Processing in Medical Imaging,* pp. 92 - 105, 2001.

[10] O.Coulon, D.C. Alexander, S. Arridge, Diffusion Tensor Magnetic Resonance Image Regularization, Med Im Analysis, vol. 8, pp. 47-67, 2004.

[11] C. Poupon, C.A. Clark, V. Frouin, J. Regis, I. Bloch, D. Le Bihan, J.-F. Mangin, Regularization of Diffusion-Based Direction Maps for the Tracking of Brain White Matter Fascicles, NeuroImage, vol. 12, pp. 184-195, 2000.

[12] O. Pasternak, N. Sochen, Y. Assaf, Separation of White Matter Fascicles From Diffusion MRI Using Φ-Functional Regularization, Proc. Intl. Soc. Mag. Reson. Med., p. 1227, 2004.

[13] D. Weinstein, G. Kindlmann, and E.C. Lundberg, "Tensorlines: Advection Diffusion Based Propagation through Diffusion Tensor Fields," *Proc. IEEE Visualization 99*, pp. 249 - 253, 1999.

[14] T.E. Conturo, N.F. Lori, T.S. Cull, E. Akbudak, A.Z. Snyder, J.S. Shimony, R.C. McKinstry, H. Burton, and M.E. Raichle, "Tracking Neuronal Fiber Pathways in the Living Human Brain," *Proc. Natl. Acad. Sci. USA,* pp. 10422 - 10427, 1999.

[15] A. Vilanova i Bartroli, G. Berenschot, C. van Pul, DTI Visualization with Streamsurfaces and Evenly-Spaced Volume Seeding, Proc. VisSym '04 Symposium on Visualization, pp.173-182, 2004.

[16] G. Grigoryan, P. Rheingrans, Point-Based Probabilistic Surfaces to Show Surface Uncertainty, IEEE Trans Visual Comp Graph, vol. 10, pp. 564-573, 2004.

[17] U. Klose, I. Mader, A. Unrath, M. Erb and W. Grodd, " Directional correlation in white matter tracks of the human brain," J. Magn. Res. Im., vol. 20, pp. 25 - 30, 2004.

[18] B.J. Jellison, A.S. Field, J. Medow, M. Lazar, M.S. Salamat and A.L. Alexander, "Diffusion Tensor Imaging of Cerebral White Matter: A Pictorial Review of Physics, Fiber Tract Anatomy, and Tumor Imaging Patterns," Am. J. Neuroradiol., vol. 25, pp. 356 - 369, 2004.

[19] S. Mori, K. Frederiksen, P.C.M. van Zijl, B. Stieltjes, M.A. Kraut, M. Solaiyappan, M.G. Pomper, Brain White Matter Anatomy of Tumor Patients Evaluated with Diffusion Tensor Imaging, Annals Neurol, vol. 51, pp. 377-380, 2002.

## VITAE

**Hans.-H. Ehricke** is a professor in the Electrical Engineering and Computer Science Department of the University of Applied Sciences Stralsund, Germany. He is head of the computer graphics lab and director of the Steinbeis Transfer Center for Image Processing and Medical Informatics. His research interests include medical imaging and virtual reality. Ehricke received a M.S. in medical informatics and a PhD in theoretical medicine from the University of Heidelberg. He is a member of the Eurographics Association and the IEEE Computer Society.

**Uwe Klose** studied physics at the University of Göttingen, Germany, and received a PhD in physics from the University of Tübingen, Germany. He is associate professor and works as a senior physicist in the Section on Experimental Magnetic Resonance of the CNS at the University of Tübingen. His research interests include advanced measurement techniques in magnetic resonance imaging and spectroscopy.

**Wolfgang Grodd** received a diploma in biology and a M.D. degree in medicine from the University of Tübingen, Germany. He has been a Postdoctoral Fellow at the Department of Radiology, University of California, San Francisco. Since 1995, he is professor of neuroradiology and head of the Section on Experimental Magnetic Resonance of the CNS at the University of Tübingen. His research interest focuses on proton spectroscopy and functional imaging of the brain.

## FIGURES

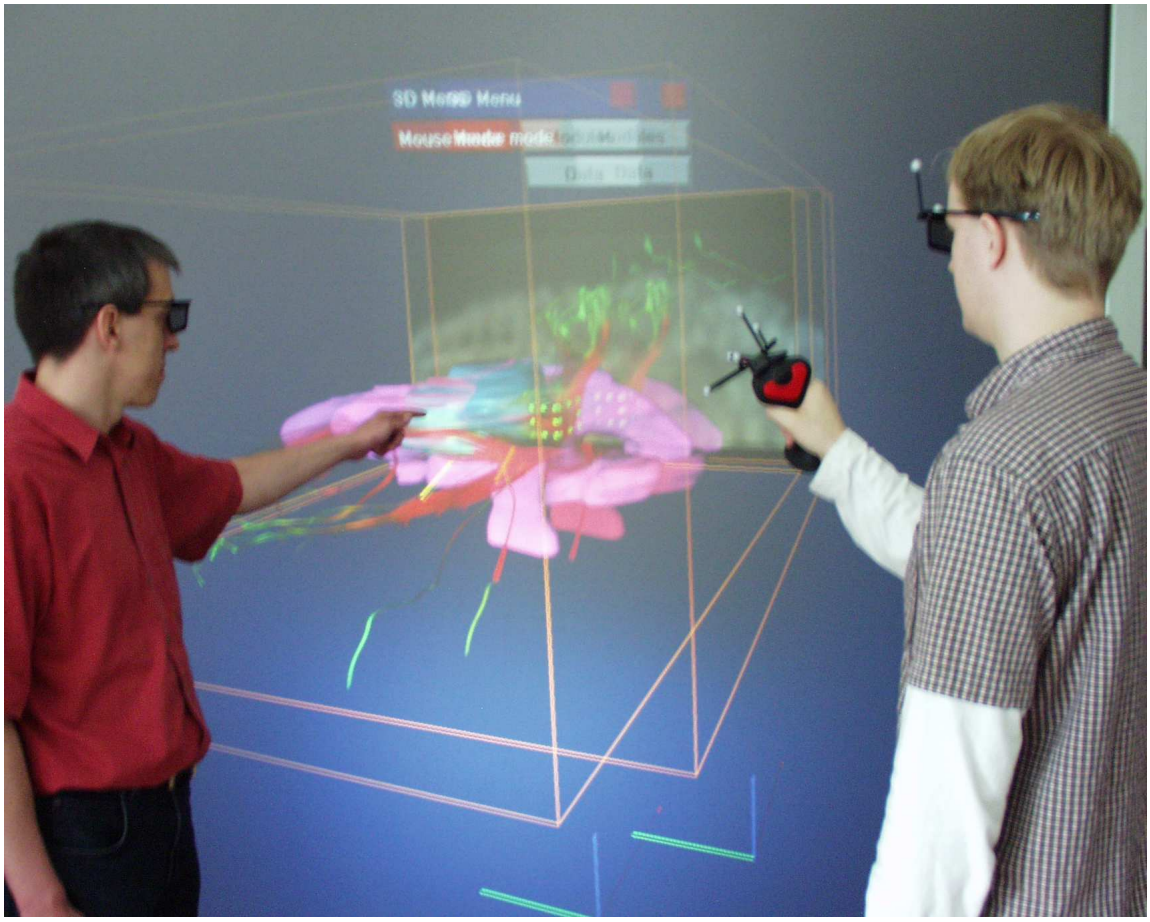

Fig. 1: Our algorithms focus on the real-time visualization of branching fiber tracts within collaborative environments. We use a passive stereos-display wall and optical tracking with a fly-stick as interaction medium.

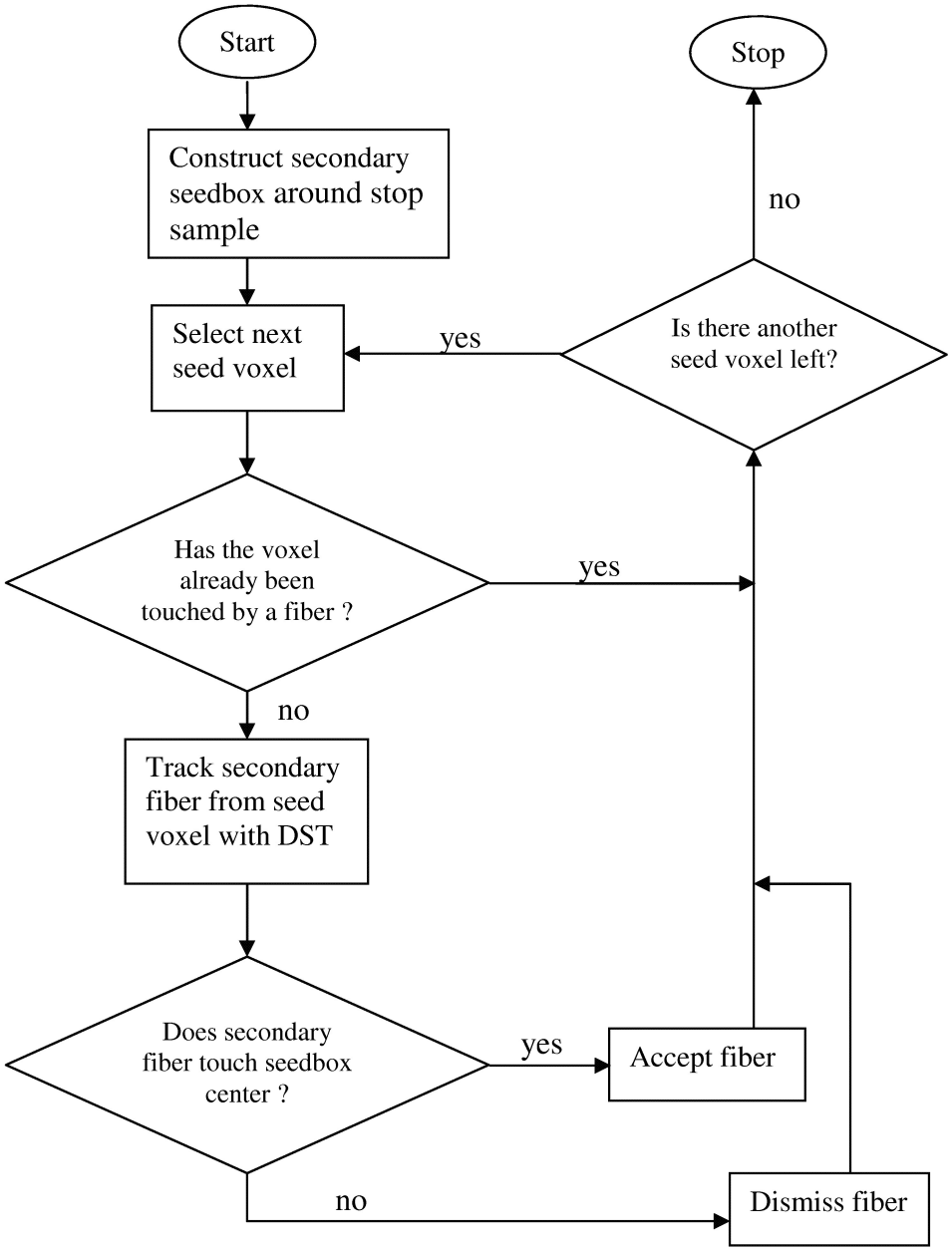


Fig. 2: Flowchart illustrating the core of the dynamic seed tracking algorithm. For each sample of the stop sample list the algorithm is executed.

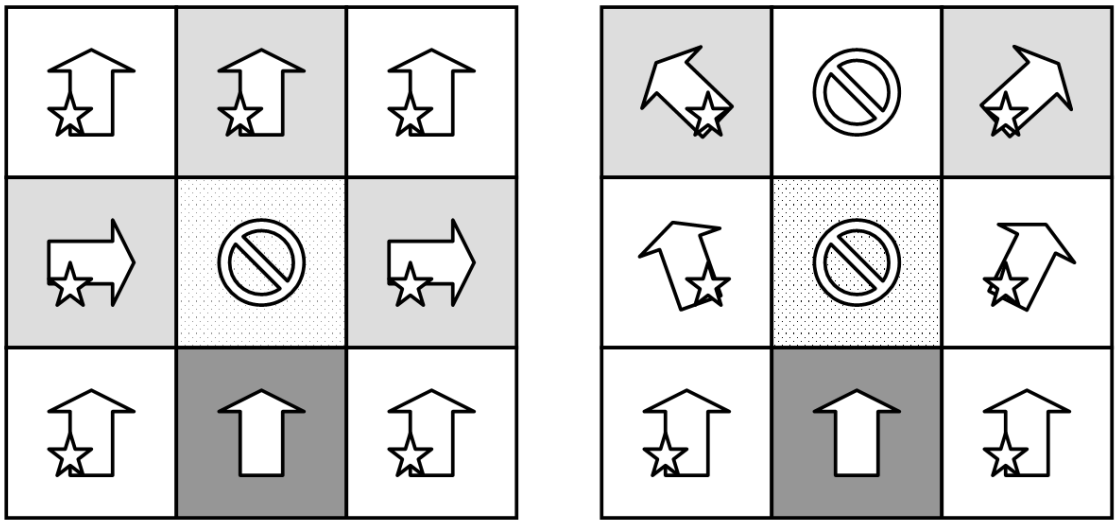

Fig. 3: Slices through dynamic seedboxes in regions with crossing (left) and branching (right) fibers. Arrows represent eigenvector orientations. Tracking of the primary fibers (dark shaded voxels) stopped at center voxels. Stars mark new seed voxels for dynamic fiber tracking. Light gray voxels represent secondary fibers which have been accepted due to their connection with the center voxel.

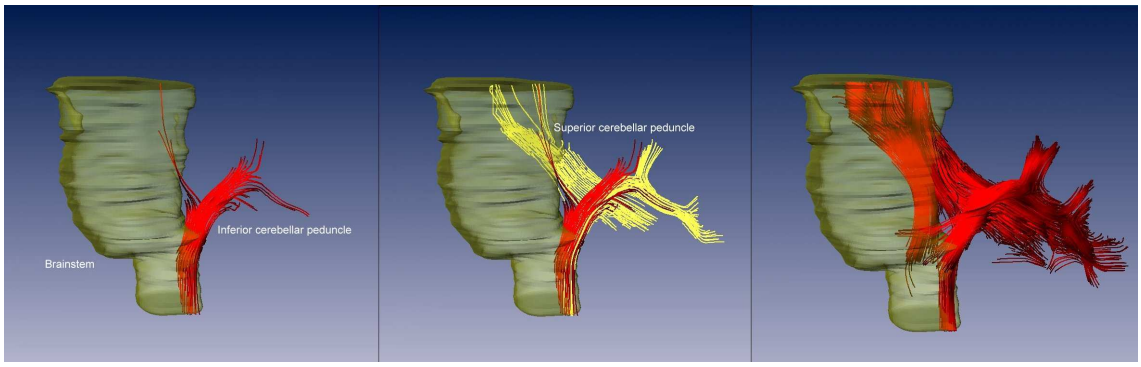


Fig. 4: Fiber tracking of cerebellar tracts without (left) and with (middle,right) dynamic seedboxes. The images show lateral views of the brainstem (surface reconstruction, gray) and the inferior cerebellar peduncle (left). The dynamic seed tracking algorithm allows streamline visualization of crossing fibers from the superior cerebellar peduncle as well as additional branches of the cerebellar peduncle (yellow). The right image was produced by accepting all fibers, originating from a secondary seedbox, whereas for the middle image only center fibers were used.

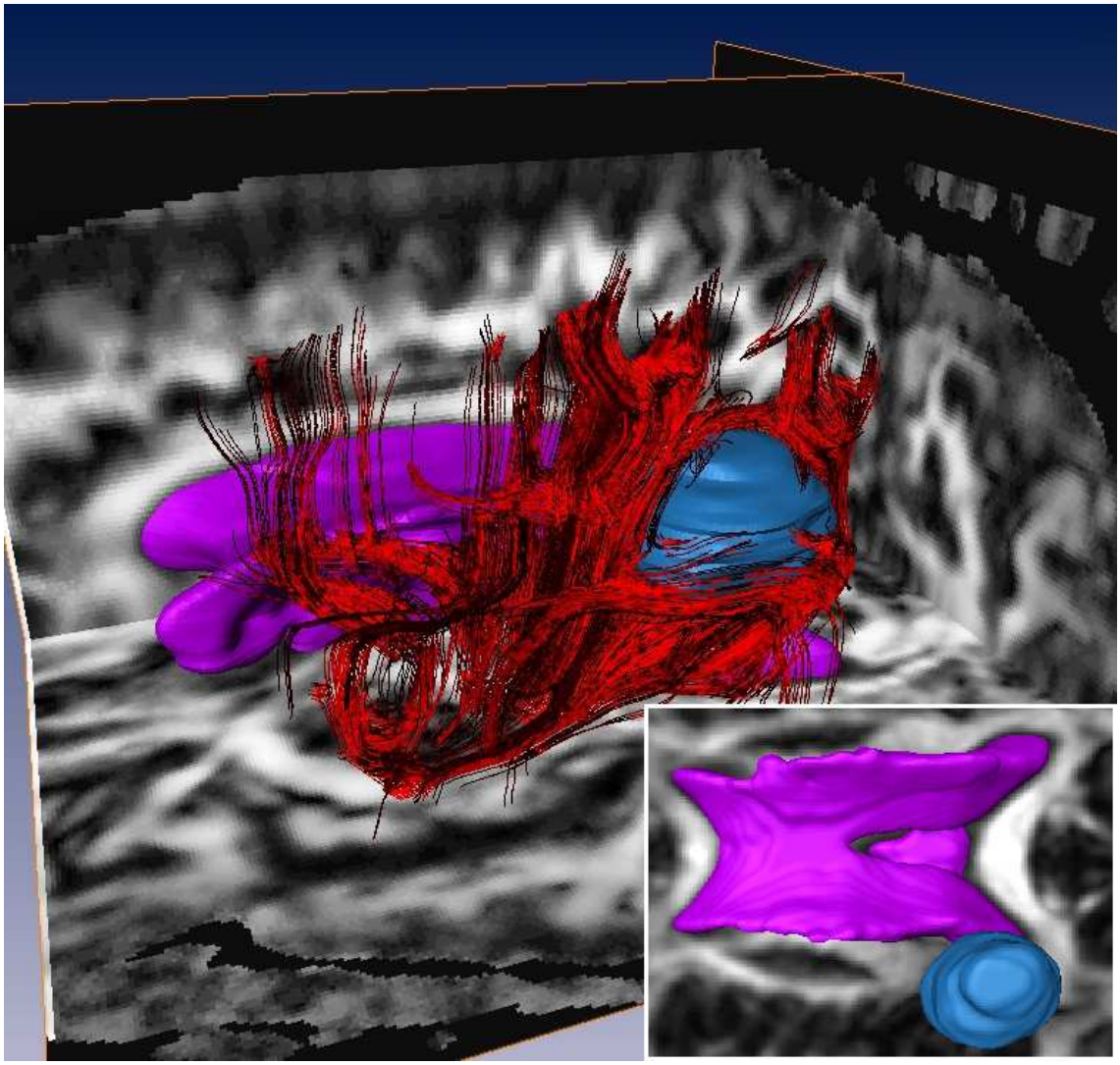

Fig. 5: Dynamic seed tracking of branching tracts around a brain tumor (cavernoma), accepting all secondary fibers originating from the seedbox. The image shows three orthogonal slices through the anisotropy data volume combined with surface displays of the ventricular system (violet) and the tumor (blue). The fibers are depicted as red streamlines. Small image: Top view without fibers.

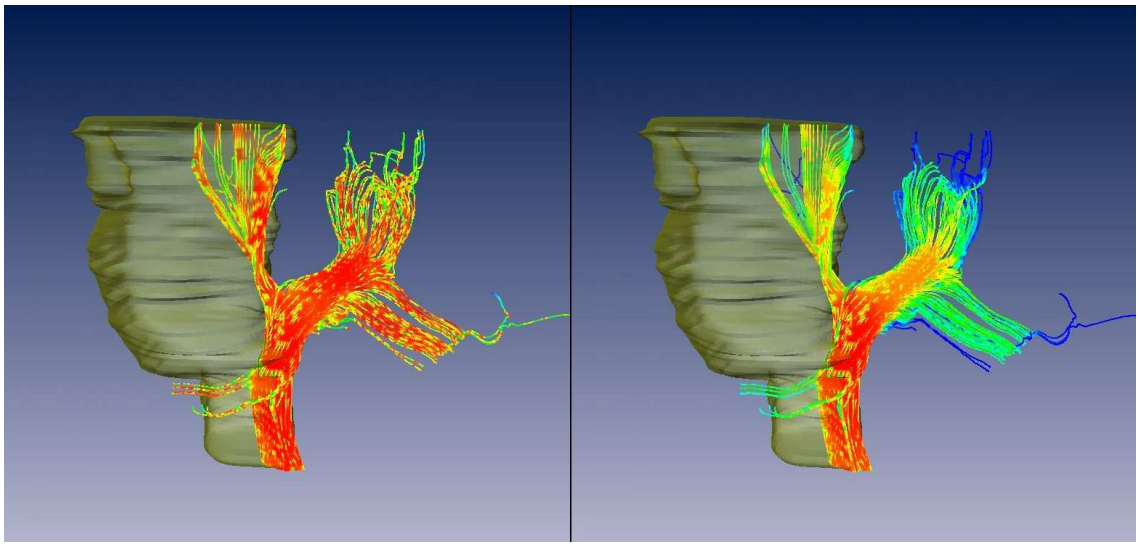

Fig. 6: Uncertainty mapping of cerebellar fibers (same dataset as fig. 4): Mapping of local probability on the basis of vector conformity (left) and conditional probability (right). A hue ramp from blue (low probability) to red (high p.) was used for colour coding. The right image allows better distinction between low and high probability fiber segments.

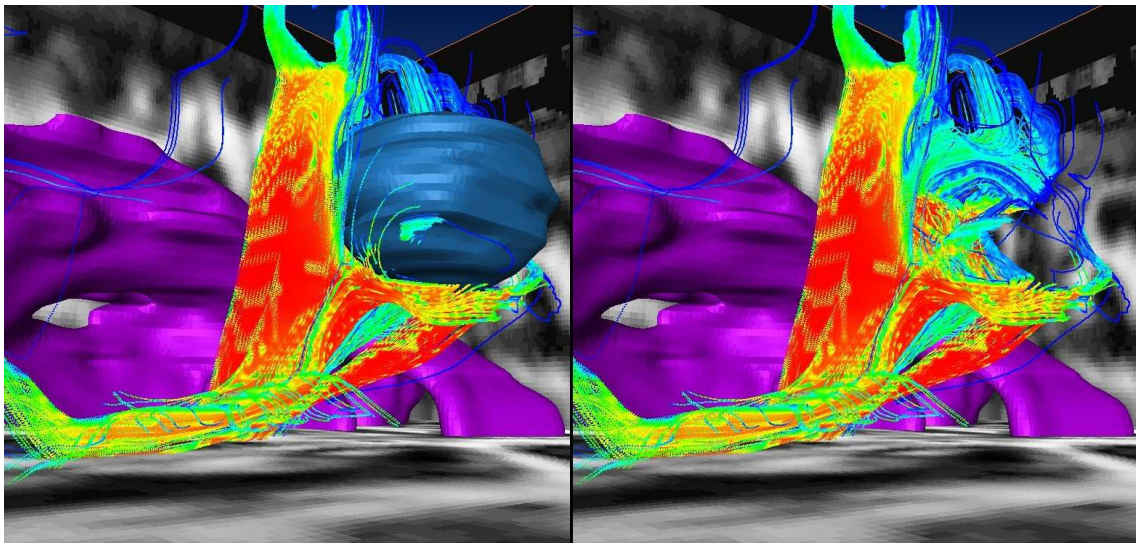

Fig. 7: Uncertainty mapping on the basis of conditional probability values computed from vector conformity and anisotropy (same dataset as fig. 5): On the right the tumor surface was removed in order to visualize fibers at its back.

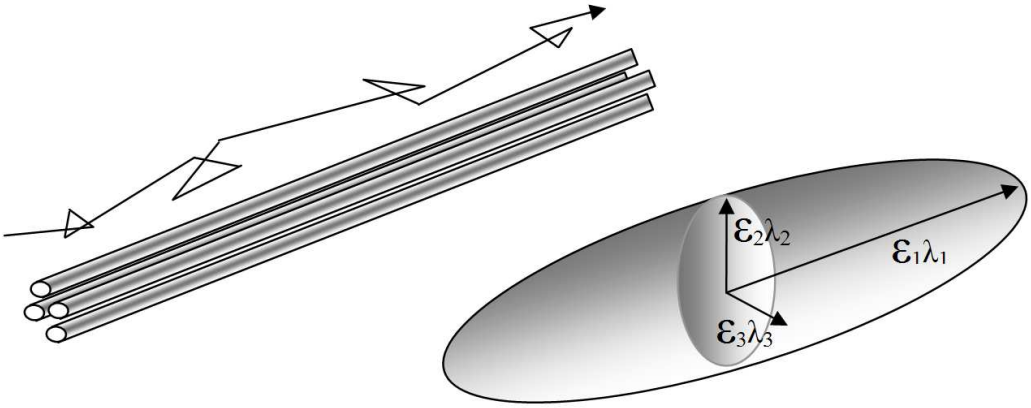


Fig. 8: Anisotropic behaviour of water diffusion within axonal fibers: Random motion of water molecules is canalized by axonal membranes and myelin sheats. The diffusion tensor may be visualized as an ellipsoid with eigenvectors $\varepsilon_i$ and their corresponding anisotropy values $\lambda_i$ (eigenvalues). The principal diffusion direction is given by the principal eigenvector $\varepsilon_1$.

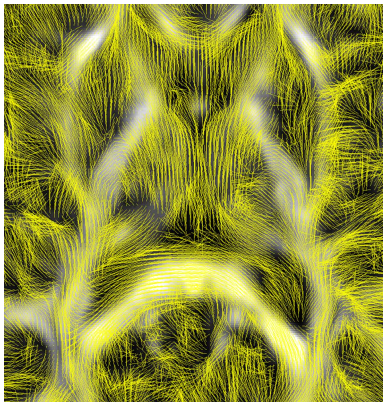

Fig.9: Two-dimensional visualization of principal eigenvectors (yellow) projected onto a slice through the volume of anisotropy values (standard deviation of eigenvalues).